Tailored fibre waveguides for precise two-axis Lissajous scanning

M. H. H. Mokhtar* **and R. R. A. Syms**

Electrical and Electronics Engineering Dept., Imperial College London, Exhibition Road, London SW7 2AZ, UK
m.mokhtar11@imperial.ac.uk

Abstract: A two-axis optical imaging system using a Lissajous scan pattern with non-integer frequency ratio is presented. A waveguide with precisely tuned mechanical resonant frequencies is constructed by dip coating two fibres with a transparent polymer. Motion is achieved by mounting a waveguide cantilever at 45° on a single piezoelectric actuator with a dual-frequency drive. Confocal signal collection is achieved using a mode-stripping detector, and feedback signals needed for frequency and phase locking are derived from intermittent reflection from an apertured mirror. The first scan axis is locked to the resonance of one of the modes, while the second scan axis is locked to the correct phase at the desired frequency ratio. Accurate acquisition of two-dimensional images is demonstrated.

OCIS codes: (060.2350) Fiber optics imaging; (120.5800) Scanners.

References and links

1. L. Giniūnas, R. Juskaitis, and S. V. Shatalin, "Endoscope with optical sectioning capability," Appl. Opt. **32**(16), 2888–2890 (1993).
2. F. Helmchen, M. S. Fee, D. W. Tank, and W. Denk, "A miniature head-mounted two-photon microscope. high-resolution brain imaging in freely moving animals," Neuron **31**(6), 903–912 (2001).
3. B. A. Flusberg, J. C. Jung, E. D. Cocker, E. P. Anderson, and M. J. Schnitzer, "In vivo brain imaging using a portable 3.9 gram two-photon fluorescence microendoscope," Opt. Lett. **30**(17), 2272–2274 (2005).
4. M. T. Myaing, D. J. MacDonald, and X. Li, "Fiber-optic scanning two-photon fluorescence endoscope," Opt. Lett. **31**(8), 1076–1078 (2006).
5. C. J. Engelbrecht, R. S. Johnston, E. J. Seibel, and F. Helmchen, "Ultra-compact fiber-optic two-photon microscope for functional fluorescence imaging in vivo," Opt. Express **16**(8), 5556–5564 (2008).
6. Y. Wu, J. Xi, M. J. Cobb, and X. Li, "Scanning fiber-optic nonlinear endomicroscopy with miniature aspherical compound lens and multimode fiber collector," Opt. Lett. **34**(7), 953–955 (2009).
7. C. M. Lee, C. J. Engelbrecht, T. D. Soper, F. Helmchen, and E. J. Seibel, "Scanning fiber endoscopy with highly flexible, 1 mm catheterscopes for wide-field, full-color imaging," J. Biophotonics **3**(5-6), 385–407 (2010).
8. Q. Y. J. Smithwick, E. J. Seibel, P. G. Reinhall, and J. Vagners, "Control aspects of the single fiber scanning endoscope," Proc. SPIE **4253**, 176–188 (2001).
9. S. Moon, S.-W. Lee, M. Rubinstein, B. J. F. Wong, and Z. Chen, "Semi-resonant operation of a fiber-cantilever piezotube scanner for stable optical coherence tomography endoscope imaging," Opt. Express **18**(20), 21183–21197 (2010).
10. T. Wu, Z. Ding, K. Wang, M. Chen, and C. Wang, "Two-dimensional scanning realized by an asymmetry fiber cantilever driven by single piezo bender actuator for optical coherence tomography," Opt. Express **17**(16), 13819–13829 (2009).
11. H.-C. Park, Y.-H. Seo, and K.-H. Jeong, "Lissajous fiber scanning for forward viewing optical endomicroscopy using asymmetric stiffness modulation," Opt. Express **22**(5), 5818–5825 (2014).
12. D. A. Roberts, R. R. A. Syms, A. S. Holmes, and E. M. Yeatman, "Dual numerical aperture confocal operation of a moving fibre bar-code reader," Electron. Lett. **35**(19), 1656–1658 (1999).
13. M. H. H. Mokhtar and R. R. A. Syms, "Resonant fiber scanner with optical feedback," Opt. Express **22**(21), 25629–25634 (2014).

1. Introduction

Because of their small size and portability, optical scanning systems based on the resonant mechanical oscillation of a fibre or waveguide cantilever in front of a lens have been of interest for many years. Applications include endoscopy [1] and biomedical imaging [2, 3]. Two methods of scanning are commonly used. In Lissajous scanning [2, 3], different frequencies are used for the x- and y-motions, with fixed amplitudes. In spiral scanning, the

#241991 Received 28 May 2015; revised 1 Jul 2015; accepted 1 Jul 2015; published 30 Jul 2015

same frequency is used, but the amplitude is varied [4–7]. Each method has its merits. A circular fibre naturally provides the degenerate resonances required for spiral scanning. However, sampling is highly non-uniform. Lissajous scanning offers greater possibilities for sampling, but requires a waveguide with non-degenerate bending modes.

In practise, the resonant frequencies of a waveguide cantilever cannot easily be specified. As a result, the shape of the Lissajous figure tends to be defined more by the characteristics of the cantilever than a desirable pattern. Even when the nearest suitable frequency ratio is chosen, operation off-resonance introduces phase shifts between drive and response [2]. Non-linear effects also introduce coupling between nearly degenerate modes, which cause the fibre to deviate further from its commanded position [8]. Without feedback, it is difficult to identify the origin of back-scattered data, so the image suffers from distortion. Some solutions have been found. Non-resonant operation has been used to minimise phase shifts [9], mechanical arrangements have been devised to adjust the resonant frequency of non-degenerate modes [2, 10, 11], and position-sensitive detectors have been used to provide feedback [8, 10]. However, these solutions do not address the key problem, namely that standard fibres are unsuitable for Lissajous scanning but it is difficult to construct an alternative.

Here, we show how a simple solution – the use of two fibres – can yield a non-degenerate system with an easily adjustable frequency ratio. In addition, we show how optical feedback may be provided to eliminate uncertainty in position. The system is based on a much older confocal scanner, which uses the same fibre to illuminate the target and receive the back-scattered signal. Dual numerical aperture operation is obtained by using the fibre core for illumination and the cladding for reception, greatly increasing the detected signal [12]. However, in its current version, the lens is surrounded with an aperture, and over-scanning provides the timing pulses needed for control [13]. Together, these techniques allow the controllable generation of Lissajous figures and accurate image reconstruction. Suitable scan patterns are described in Section 2, a method of preparing frequency-tailored waveguides in Section 3, the experimental scanning system in Section 4, and results in Section 5. Conclusions are drawn in Section 6.

2. Scan pattern selection

Lissajous figures are plane curves obtained when the x- and y-co-ordinates both vary harmonically, but at unequal rates. Here we consider figures defined by $[x, y] = -[\sin(r\omega t), \cos(\omega t)]$, where ω is angular frequency, t is time and r is a fixed frequency ratio. Well-known results are obtained when r is integer. Segments of any such figures do sweep across useful regions of the x-y plane, but large values of r are required to obtain dense sampling. More practical results are obtained when r is no longer integer, but still rational. We consider the family obtained when $r = m + 1/n$, with m and n both integers. All such figures must repeat after finite time, since x and y sweep out a whole number of cycles when $\omega t = 2n\pi$. To avoid coupling between nearly degenerate modes, we ignore the case when $m = 1$, and consider instead $m = 2$. Figures 1(a) and 1(b) show Lissajous figures for $n = 2$ and $n = 3$, respectively. In the former case, the curve retraces itself, while in the latter a closed loop is obtained.

The same behaviour is obtained for larger values of n: symmetric closed loops are only obtained when n is odd. Furthermore, odd values provide a higher density of scan lines. For example, Fig. 1(c) shows the Lissajous figure for $n = 15$ (corresponding to $r = 2.067$). As n rises, the frequency ratio tends to 2. In this range, different figures may easily be obtained using a dual-mode system with moderate bandwidth. The density of scan lines and the spacing of regular sampling points are both clearly non-uniform, and lowest in at the centre of the field-of view (FOV). There are two approaches to increasing resolution. Firstly, the value of n can simply be increased, as previously discussed; the line density then increases proportionally. Secondly, additional scans can be carried out with the same n, but with deliberately applied phase shifts. The grey lines in Fig. 1(b) have been generated using phase shifts of ± 18° applied to the x-drive; clearly, their effect is to treble the apparent line density.

To illustrate this, we use a target object consisting of the character '@', printed on paper in 3 pt Calibri using an HP LaserJet Pro M401dn. Figure 2(a) shows an optical microscope

#241991 Received 28 May 2015; revised 1 Jul 2015; accepted 1 Jul 2015; published 30 Jul 2015

photograph of this target, converted into a 256 x 256 pixel image. A simulated scan was carried out in MATLAB, by calculating the x- and y-co-ordinates of a single cycle, and sampling the brightness z of the nearest pixel at 1106 points per fast cycle. The (x, y, z) values were mapped onto a regular grid as a new set of data (X, Y, Z) using the linear MATLAB griddata function, and the image was then reconstructed using the filled contour function contourf. Figure 2(b) shows the result, which is clearly an excellent representation of Fig. 2(a).

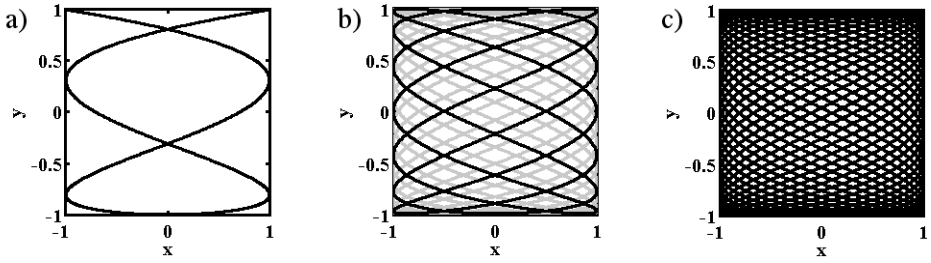

Fig. 1. Ideal Lissajous curves for m = 2 and a) n = 2, b) n = 3 and c) n = 15; also shown in grey are additional lines obtained by scanning with deliberate phase shifts applied to the x-drive.

Lissajous sampling is, however, extremely sensitive to phase deviations, which cause errors in the origin of the sampled data. To illustrate this, we consider the effect of sampling using the modified trajectory [x', y'] = -[sin(rωt + ϕ), cos(ωt)], but reconstructing using the assumed trajectory [x, y]. Figure 2(c) shows the image obtained from Fig. 2(a) with ϕ = 4°. The phase error has caused block-wise shifts in image data in the x-direction, which introduce a characteristic castellated appearance. For slightly larger errors, the image is unrecognisable. The effect is generally not remarked upon in the literature. This is surprising, when one considers that phase shifts can only be avoided in a mechanically resonant system using a cantilever whose two bending modes lie in the precise ratio r. If this is not the case, one mode may be resonant, but the other must necessarily be off-resonance. In an under-damped system, this mode will inevitably be out of band, and require large correction to the amplitude and phase of its drive. A simple method of constructing waveguide cantilevers whose primary resonances lie in a ratio close to 2 is therefore required. Here we demonstrate a simple and reproducible approach based on conventional optical fibre.

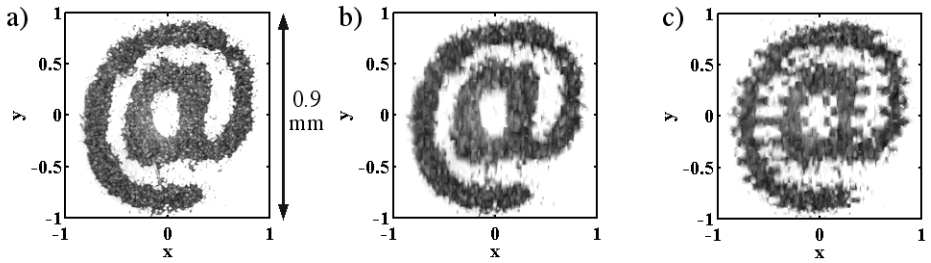

Fig. 2. a) Experimental target object; b) and c) images reconstructed following simulated Lissajous scanning with n = 15, without and with a phase error of 4°.

3. Frequency tunable waveguide cantilevers

Standard theory gives the angular resonant frequency ω of the lowest-order bending mode of a cantilever beam as $\omega = (\alpha/L^2)\sqrt{(EI/\rho A)}$. Here L, A and I are the length, cross-sectional area and second moment of area of the beam, ρ and E are the density and Young's modulus of the beam material, and α = 3.516 is a constant found by numerical solution of the beam-bending equation. For a beam with second moments I_{xx} and I_{yy} about the two principal axes we would expect high and low frequencies ω_H and ω_L, in the ratio $\omega_H/\omega_L = \sqrt{(I_{yy}/I_{xx})}$. For a cylindrical fibre of radius r, $I_{xx} = I_{yy} = \pi r^4/4$ and $\omega_H/\omega_L = 1$. However, for two fibres attached together as

#241991 Received 28 May 2015; revised 1 Jul 2015; accepted 1 Jul 2015; published 30 Jul 2015

shown in Fig. 3(a), $I_{xx} = 2(\pi r^4/4)$, while $I_{yy} = 2(\pi r^4 + \pi r^4/4)$. In this case, we obtain $\omega_H/\omega_L = \sqrt{5}$, or 2.236. This ratio is already close to the desired value, and can be controllably reduced using further fillet of material that preferentially adds mass and stiffness near x = 0 as shown in Fig. 3(b). For example, for a full fillet as shown in Fig. 3(c), with Young's moduli E_1 and E_2 for the fibre and fillet material, such that $R = E_2/E_1$, we obtain $\omega_H/\omega_L = \sqrt{\{[5 + R(16 - 5\pi)/2\pi]/[1 + R(16 - 3\pi)/6\pi]\}}$. For R = 1, this reduces to $\omega_H/\omega_L = 1.934$, below 2. However, additional material can be added near A and A' to increase the effect. We have found this necessary for the polymer fillers investigated, which have small Young's moduli.

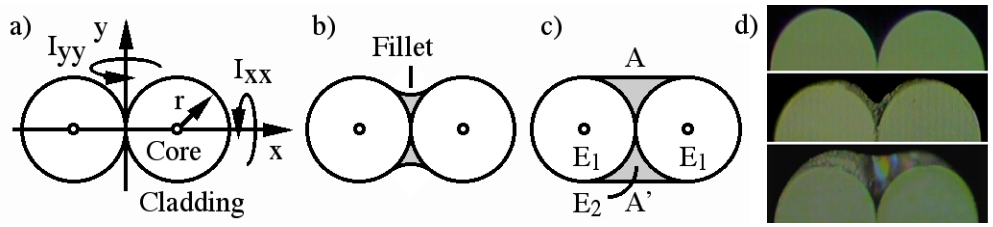

Fig. 3. Ideal cross-section of dual-core waveguide with a) no, b) partial and c) full polymer fillet; d) experimental guide cross-sections after different numbers of polymer coats.

A suitable waveguide may be constructed from a pair of optical fibres as shown in the cross-sectional photographs of Fig. 3(d). All that is required is a system capable of adding material by dip coating with a transparent liquid polymer such as varnish, as shown in Fig. 4(a). We assume for convenient handling that the fibres are already embedded in a plastic matrix (for example, in a ribbon). The matrix is first stripped to expose the cladding for a length of ≈10 cm, and the ends are cleaved (1). At this point, the fibres will be widely separated (in a ribbon, by 300 μm). This length is then dip-coated with diluted varnish, which is allowed to dry. As the fibres emerge from the liquid, capillary forces at the meniscus align them accurately together (2). The composite waveguide is then re-coated, this time using undiluted polymer so that capillary action fills in the desired fillet (3), and again allowed to dry. The cleaved fibre ends are then exposed by dip coating a final time in solvent (4). Multiple coats may be applied to modify the cross-section controllably, and the resonant frequencies of the modes may be identified by exciting motion under a microscope. However, care is needed to ensure that the fibres are closely spaced and parallel, and that the waveguide is rigidly attached as a built-in cantilever.

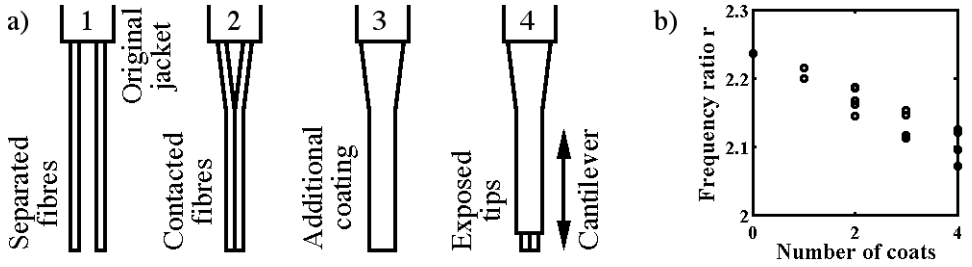

Fig. 4. a) Procedure for waveguide cantilever construction by dip coating; b) variation of the frequency ratio r with the number of polymer coats.

Figure 4(b) shows the variation of the frequency ratio r with number of dip-coating cycles, obtained using Humbrol Gloss Cote varnish (poly butyl methacrylate, PBMA) at a pull rate of 2 mm/sec. Because the Young's modulus of PBMA ($E = 1.37 \times 10^9$ N/m^2) is much lower than that of silica ($E = 73.1 \times 10^9$ N/m^2), the modification to r is small. However, there is a steady downward trend in r from the value of $\sqrt{5}$, and r-values down to 2.07 can be obtained for thick coats that are fully cured (as in the lower of Fig. 3(d)). We have increased this range using poly methyl methacrylate (PMMA, $E = 3.1 \times 10^9$ N/m^2), and would expect further increases using sol-gel glass (E approaching that of silica).

#241991 Received 28 May 2015; revised 1 Jul 2015; accepted 1 Jul 2015; published 30 Jul 2015

The reproducibility of dip coating has been verified over decades of experience in applications such as lithography. Of course there is some variation, and this increases with the number of coats. However, we have fabricated many cantilevers (Fig. 4(b) shows data from 17) and the frequency ratio is still quite precise. For 4 coatings, the ratio is 2.097 ± 0.025, a variation of ± 1.2%. This value is small enough to lie within the pass-band of cantilever resonators with Q-factors of ≈100. For PMMA, the comparable value is 2.015 ± 0.05.

Although [10] and [11] achieve the same aim, we deliberately developed our frequency ratio tuning method as an alternative to the time-consuming procedures in these works. Although its tuning range is inherently smaller, it generates frequency ratios based on highly predictable integer values, and results in composite waveguides with uniform cross-section, so r is independent of cantilever length. Finally, it is capable of mass-production using simple equipment. As a result, we believe it to be considerably simpler and more controllable.

4. Experimental scanning system

Tailored fibre cantilevers may be used as the basis of a confocal scanning system as shown in Fig. 5(a). The two modes are excited by mounting the waveguide at 45° on a single piezo-electric transducer using a Vee block as shown in Fig. 5(b), and using a dual-frequency drive to excite both modes together. Of course, it is unlikely that the exact ratio of resonant frequencies will be achieved. However, one drive frequency is chosen to operate the low mode exactly at resonance. Provided the second drive frequency lies within the bandwidth of the high mode, this may be excited with minor phase and amplitude corrections. Feedback signals are needed to allow control of the frequency of the first motion and the phase of the second. Feedback signals can be obtained using a thin aperture with a square opening in front of the lens, which provides large back-scattered timing pulses from the scan extremities [13].

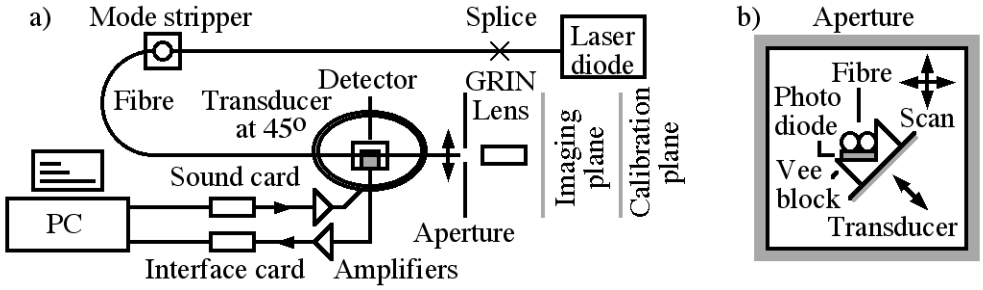

Fig. 5. Arrangements for a) optical coupling, mechanical excitation and signal detection and b) waveguide mounting and provision of feedback.

Experiments were carried out with the arrangement in Fig. 6(a), which shows the fibre and photodiode supported on a Vee block on a piezoelectric disc transducer. The light source was a 635 nm fibre-coupled laser diode, operating at 4.5 mW power. The output fibre was spliced to a length of fibre waveguide, prepared from two fibres with 8 μm diameter core and 125 μm diameter cladding. A mode stripper was used at the input. Target illumination was achieved by focussing the light emerging from the fibre core using 1.8 mm diameter, 0.23-pitch anti-reflection coated GRIN lens. Back-scattered light was collected over a larger numerical aperture in the fibre cladding and passed to a mode-stripping detector (a surface-mount PIN photodiode, connected to a transimpedance amplifier). The fibre was glued to the photodiode, which was mounted on a plastic V-block to achieve the correct orientation with a cantilever length of 30 mm. The V-block was attached to a 50 mm diameter piezoelectric diaphragm, driven via an operational amplifier. The scanning fibre and the lens were mounted on an x-y-z stage to allow transverse and axial alignment. However, in a packaged module, the fibre can be mounted on two V-blocks, one attached to a fixed land and the other to the piezoelectric transducer. The GRIN-lens can be similarly mounted. Since the fibre cross-section self-aligns to each V-block, there are no significant alignment issues. The aperture was a crossed pair of 1.5 mm wide slots in photo-etched steel, which were positioned in front of the lens using a

#241991 Received 28 May 2015; revised 1 Jul 2015; accepted 1 Jul 2015; published 30 Jul 2015

further x-y-z stage. Differences in the axial position of the slots resulted in reflected pulses of different heights, allowing the two feedback signals to be distinguished. Scan patterns were observed in a calibration plane, and images were acquired from targets closer to the lens.

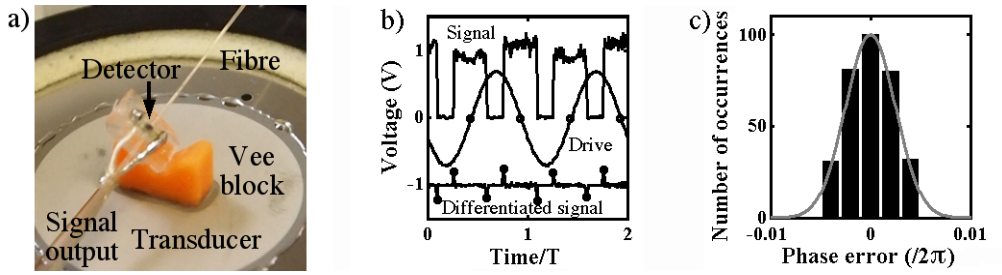

Fig. 6. a) Mounting of fibre and detector; b) time variation of the drive, signal and differentiated signal for the resonant mode, with points indicating timing edges and extracted zero-crossings; c) histogram of phase error.

The drive signal was generated using a sound card sampling at 44.1 kS/sec. The drive and the detected signal were both sampled using an interface card at an aggregate rate of 250 kS/sec. The controller was implemented using MATLAB. Data was acquired over a number of cycles, the pulse centres were extracted using software, and control algorithms used to apply new scan parameters in an iterative cycle. For the resonant mode, the frequency was first adjusted for a 90° phase lag between the pulse position (which indicates the maximum fibre excursion) and the drive, and the amplitude was then adjusted to reduce the pulse length to a practical value as described in [13]. Figure 6(b) shows the time variation of the drive and back-scattered signal, with the system drive only on the resonant mode for clarity. The signal contains large timing pulses scattered from the aperture, with much smaller back-scattered data between. Numerical differentiation allows identification of the rising and falling edges of the pulses, and extraction of the zero-crossings of the drive.

The amplitude and phase errors may also be extracted from the timing data. Both show excellent stability. Figure 6(c) shows a histogram of phase error taken from a data sequence containing 340 consecutive periods. The data has been matched to a Gaussian distribution, with standard deviation of $\sigma = 0.0025 \times 2\pi$ radians, or 0.9°. This value is almost exactly the standard deviation of the digitally generated drive voltage. Consequently, the phase jitter can be ascribed to sampling, and could be reduced by faster electronics. However, the phase error is already less than a quarter of the value in the example of Fig. 2(c), and unlikely to affect the image. For the off-resonant mode, the frequency was set to the desired value, the phase was then adjusted to correct for the measured deviation from a 90° phase-lag, and the amplitude was then adjusted. The system was then allowed to settle before the next iteration.

5. Experimental results

The results that follow were obtained using a cantilever with high and low resonant frequencies of $f_H = 234.1$ Hz and $f_L = 113$ Hz (so $r = 2.072$). Figures 7(a) and 7(b) show the normalised frequency responses of the two modes. The experimental data (points) have been matched to a mass-spring damper model (lines), with damping factors of $\zeta = 0.005$ (high mode) and $\zeta = 0.014$ (low mode). The bandwidth of the high mode is easily sufficient for Lissajous figures with $n = 12$ to $n = 16$. We have verified that this is the case, and measured the correction required to adjust for off-resonance phase shifts. The experimental values (points) are shown compared with the model in Fig. 7(c); there is clearly good agreement.

#241991 Received 28 May 2015; revised 1 Jul 2015; accepted 1 Jul 2015; published 30 Jul 2015

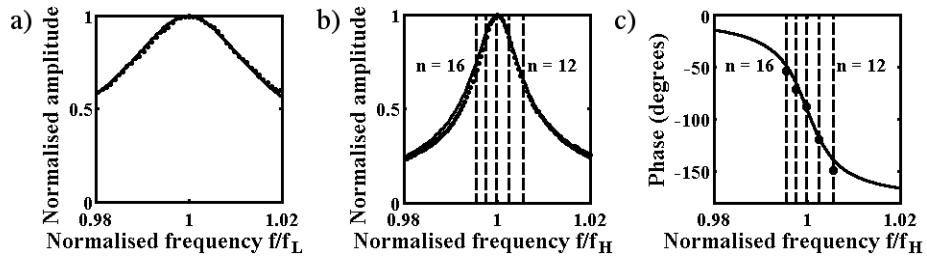

Fig. 7. a) and b) normalised frequency responses of low and high modes; frequency variation of phase for the high mode. Points are experimental, lines are theoretical predictions.

Figures 8(a) and 8(b) show line scans obtained in the calibration plane by driving the transducer at the two resonant frequencies separately at voltages of 1.06 V and 2.86 V, demonstrating that linear, orthogonal scan lines may be obtained, without the ellipticity characteristic of near-degenerate modes. Figure 8(c) shows the Lissajous figure for n = 15 obtained by driving the transducer with the two frequencies together, with the necessary phase correction applied. The agreement with Fig. 1(c) is excellent.

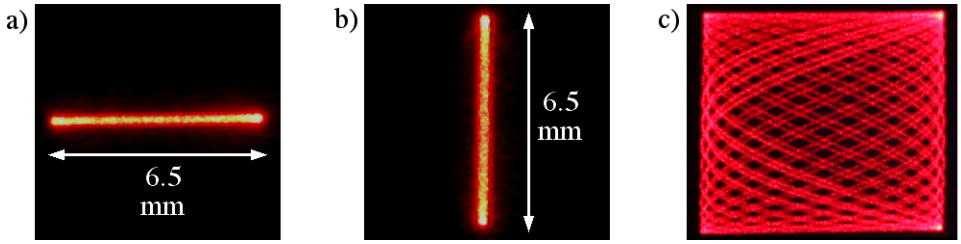

Fig. 8. a) and b) experimental line scans in the x- and y-directions; c) experimental Lissajous pattern with n = 15.

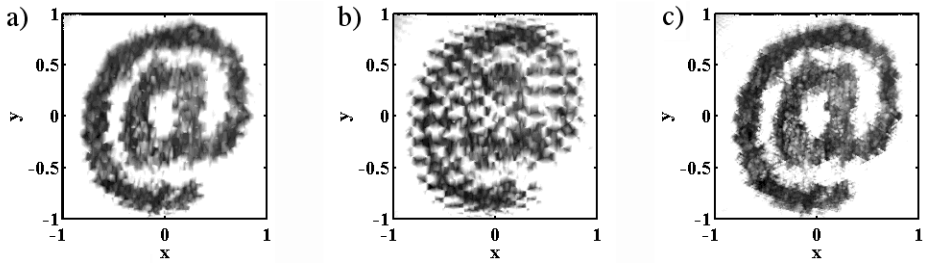

Fig. 9. Images reconstructed from experimental data acquired by Lissajous scanning with n = 15, a) with no phase error, b) with a phase error of 4°, and c) from three scans with deliberate phases offsets of –4°, 0° and + 4°.

Imaging was carried out using the experimental target, Fig. 2(a). Figure 9(a) shows the image reconstructed using back-scattered data from a single cycle, which has been processed using the previous algorithm, but with thresholding to remove reflection from the fibre facet and to limit spikes. Figure 9(b) shows the image without phase correction, and hence with a phase error of 4°. The agreement between these figures and the simulations in Figs. 2(b) and 2(c) is remarkable, and shows that phase-locking of the modes can allow faithful image acquisition. In each case, the acquisition time is $T = n/f_L = 0.133$ sec. This corresponds to a frame rate of 7.5 Hz, which could easily be increased by reducing the cantilever length.

The optical resolution is mainly determined by the large spacing of the scan lines. Here, the worst case can be found from the separation at the image centre and field of view as 42 μm. This value can be improved using multiple scans with different phase offsets, as described earlier. Figure 9(c) shows an image reconstructed from three scans with phase offsets of zero and ± 4°. The resolution has clearly improved, to an estimated value of 14 μm.

#241991 Received 28 May 2015; revised 1 Jul 2015; accepted 1 Jul 2015; published 30 Jul 2015

6. Conclusions

We have demonstrated highly controllable Lissajous scanning in a dual numerical aperture confocal resonant fibre scanner. A waveguide with mechanical resonant frequencies in a ratio close to 2 was prepared by dip-coating two fibres, and mounted at 45° on a single transducer driven with a composite signal. The method of waveguide construction is compatible with many fibre types. Alternative coating materials such as sol-gel glass could be used to improve mechanical properties. Feedback from an aperture was used to lock the frequency of one drive signal to the resonance of one mode, and to adjust the phase of the other drive signal. Accurate control of the fibre position then allowed precise generation of Lissajous figures, and confocal collection of back-scattered signals provided efficient sampling of image data.

#241991 Received 28 May 2015; revised 1 Jul 2015; accepted 1 Jul 2015; published 30 Jul 2015